Wood Science and Technology (2025) 59:79
https://doi.org/10.1007/s00226-025-01680-4

ORIGINAL

Modelling and validation of wood permeability: combining fractal theory with mercury intrusion porosimetry method

Zhipeng Zhu[1] · Feifan Lv[1] · Jiajun Lv[1] · Riwei Huang[1] · Chiyang Mao[1] · Yingchun Cai[1] · Wanli Cheng[1] · Antoni Sánchez-Ferrer[2] · Jingyao Zhao[1]

Received: 18 December 2024 / Accepted: 5 June 2025

Abstract

The permeability of wood materials significantly affects wood modification, drying and further processing of wood-based building materials, and there is a need for a better understanding and evaluation of the permeability of wood materials. This paper presents a novel method for estimating the macroscopic permeability in wood by combining mercury intrusion porosimetry (MIP) data with the fractal theory. The characterization of wood's structural parameters through MIP provides essential geometric data for the subsequent modelling process. A computational model for permeability was established based on principles of fractal geometry and seepage flow theory. This model aimed to elucidate the relationship between the structural characteristics of wood and its permeability behaviour. By deriving an explicit expression for permeability, the model incorporated critical structural parameters, e.g., minimum and maximum pore size, pore size distribution, porosity, fractal dimension, and the fractal dimension associated with tortuosity. The permeability of the three wood species studied, i.e., Scots pine, white birch, and oak, was 28.6, 13.6 and 1.4 mD, respectively. To validate the model, the calculated permeability values were compared with experimentally measured data, showing a strong correlation and confirming that the model accurately reflects the permeability behaviour of wood based on its structural characteristics. Notably, the model demonstrated the effectiveness of utilizing MIP data in conjunction with fractal theory, thus, the computational efficiency of this method significantly surpassed that of traditional numerical simulations, which allowed a better understanding of the interplay between structure and permeability in wood.

Extended author information available on the last page of the article

Published online: 08 July 2025

Introduction

Wood is a solid foam composite material that combines amorphous and crystalline domains from three biopolymers, i.e., cellulose, hemicelluloses and lignin, and is one of the most sustainable options for carbon sequestration. Its excellent strength-to-weight ratio and processability contribute to its widespread use as a construction material (Zhu et al. 2024b). Wood permeability refers to the ease with which fluids move through wood under a pressure gradient and is affected by the porous structure. It has a direct impact on the wood modification, drying and further processing of wood-based building materials (Zheng et al. 2024). Moisture and air diffusion, which is governed by Fick's law, significantly influence the overall energy consumption of buildings (El Assaad et al. 2023). Therefore, predicting the permeability of wood-based materials accurately is essential for assessing thermal and physical stability, optimizing building energy efficiency, and enhancing occupant comfort (Portal et al. 2013; Lü et al. 2017; Zhang et al. 2022; Sanchez-Ferrer et al. 2023; Zhu et al. 2024a).

Permeability is a key property parameter that quantifies the migration of fluids (liquid or gas) within a material (Rahiminejad et al. 2024). Many researchers have explored wood permeability using various experimental techniques and theoretical models. The experimental approach remains the fundamental method for researching wood permeability, serving as the evaluation standard for simulation results (Tarmian and Mastouri 2018; Jang et al. 2020; Sanchez-Ferrer et al. 2023). Despite variations in devices and materials, the underlying principles for measuring permeability are consistent. Typically, water flow or velocity is measured using sensors under controlled pressure conditions, and permeability is subsequently calculated using Darcy's or Poiseuille's law. For instance, Ai et al. created a gas permeability detector utilizing numerical inverse analysis and established a related model to investigate how structure impacts permeability (Ai et al. 2017a, b; Di Canto et al. 2023). By employing X-ray computed tomography technology to monitor fluid flow behaviour in cork, the permeability of wood can be briefly estimated based on Darcy's law (Burridge et al. 2021; Acosta et al. 2023). In addition to traditional methodologies, Multon et al. recently utilized the relationship between moisture content, capacitance and resistance measurements to indirectly calculate permeability (Multon et al. 2022). Furthermore, Marynowicz et al. used thermal imaging to record the surface temperature of wood samples, enabling the reconstruction of the moisture frontline, from which permeability and diffusivity were inferred based on capillary permeability principles (Marynowicz and Kucharczyk 2021).

Despite a series of experimental tests, the quantitative evaluation and prediction of wood permeability remains challenging. This difficulty arises from the limitations in the accuracy of experimental facilities and predictive models, which are often inadequate for the complex conditions inherent in wood systems. Establishing a clear relationship between structural and permeability characteristics through traditional methods can be particularly demanding. However, this limitation can be effectively mitigated by supplementing experimental results with numerical simulations. Permeability can be determined by constructing a model that accurately describes the process of water flow, mirroring the actual migration of water within the material. All model parameters, e.g., inlet and outlet pressure, dynamic viscosity, and porosity, are

established through virtual parameter assignments (Merlier et al. 2019; Li et al. 2020; Brozovsky et al. 2023; Hu et al. 2023).

Currently, theoretical approaches primarily encompass numerical simulation and analytical calculation. In the case of numerical simulation, the equations that describe liquid migration are integrated into the structural framework for computational analysis. For example, Kvist et al. integrated X-ray computed tomography with lattice Boltzmann simulations to assess permeability and diffusion characteristics in wood subjected to blast treatment (Kvist et al. 2017, 2020). Zhao et al. employed the Navier-Stokes equations to model liquid movement and evaluate macroscopic permeability in wood structures (Zhao et al. 2023). However, this approach needs substantial computational resources, even for small samples, and full-scale seepage simulations have yet to be achieved. Additionally, controversies persist regarding the selection of representative elements, grid discretization, and boundary condition settings (Dang Mao et al. 2021). In contrast, analytical methods often treat the material structure as a collection of approximately parallel capillary tubes with varying diameters. Based on fractal and seepage flow theories, the flow rate across a given section can be calculated using an equivalent geometric model, from which permeability is subsequently derived. Unfortunately, research in this area specific to wood is relatively scarce, although it has been more extensively explored in other porous materials. Yuan et al. proposed an analytical model for the apparent gas permeability of tight porous media, applying fractal theory to mathematically characterize the distribution of capillary diameters and their tortuosity (Yuan et al. 2016). Yu et al. estimated sandstone permeability using SEM images based on fractal principles, establishing a correlation between the microscopic characteristics of sandstone porosity and its macroscopic permeability through image identification techniques (Yu et al. 2019). Similarly, Rezaeyan et al. utilized fractal theory to predict fluid flow regimes, permeability, and diffusivity in rock based on multi-scale pore characterization (Rezaeyan et al. 2022). These studies demonstrate the feasibility of calculating material permeability using fractal theory.

Fractal geometry, introduced by Mandelbrot in the 1970s, serves as a framework for explaining characteristics such as irregularity, instability, and complex structures (Hargittai 2024). Fractals are defined as objects whose constituent parts exhibit self-similarity to the whole, differing only in the scale. It has been demonstrated that wood systems, including various wood materials, can be effectively described using fractal principles (Li et al. 2016). In recent years, fractal theory has been used to quantitatively describe the pore structure in porous materials, however, its implementation in the study of wood, an inherently complex porous material, has not been extensively reported. According to the previous research results, it is feasible to predict permeability through the combination of mercury intrusion porosimetry (MIP) and fractal geometry (Zhao et al. 2020). Additionally, the final mathematical expressions for permeability derived from fractal models tend to be implicit, with unclear parameter interpretations. This lack of clarity hampers further investigation into the relationship between structural characteristics and material properties.

This paper presents a novel method for estimating macroscopic permeability in wood by integrating MIP data with fractal theory. Initially, the pore structure parameters of the wood were characterized and analyzed using MIP. Subsequently, a perme-

ability model was constructed based on fractal and seepage flow theories. An explicit expression for permeability was then proposed and validated through experimental results, and the influence of various factors on permeability was discussed.

Materials and methods

Material preparation

Three wood species were studied from Heilongjiang Province, China: Scots pine (*Pinus sylvestris*), oak (*Quercus mongolica*) and white birch (*Betula platyphylla*). The oven-dried densities of these species were measured at 450 kg/m³, 600 kg/m³, and 737 kg/m³, respectively, by heating all samples in an oven at 103 °C until constant weight, then removing and allowing them to cool to room temperature in a desiccator (0% RH). For permeability measurements, cylindrical sapwood samples with a diameter of 25 mm and a thickness of 5 mm in the radial direction were selected, ensuring the absence of significant visible defects. Following permeability testing, small samples of $5 \times 5 \times 5$ mm^3 were cut from the original specimens for MIP experiments, thereby minimizing experimental errors associated with wood variability. To ensure the reliability of the data, each test for each wood species was repeated three times.

Mercury intrusion porosimetry (MIP) experiments

A mercury porosimeter AutoPore IV 9500 (Micromeritics Instrument Corporation, USA) was used to assess the pore structure characteristics of the samples, including pore volume, porosity, and pore size distribution. Initially, the oven-dry specimens were placed within a sealed chamber to ensure isolation from environmental factors. The measurement process started with a gradual increase in pressure, ranging from 0.1 psia to 60,000 psia (from 689 Pa to 414 MPa), while the sample was submerged in non-wetting mercury. To ensure accurate measurements, an equilibrium time of 10 s was established for each pressure increment. The pressure increase rate was automatically adjusted by the advanced control system of the instrument, which employed slower rates at lower pressure levels to enhance precision during the mercury intrusion. As the pressure increased, mercury progressively infiltrated the sample, moving from larger voids to smaller ones, thus allowing for a comprehensive analysis of the wood's internal structure. Each scan cycle lasted approximately 60 min, during which the amount of intruded mercury was recorded. After completing the scans, the pore volume was calculated based on the volume of mercury that penetrated the samples. The pore size distribution was subsequently determined using the Washburn equation as Eq. 1, which establishes a relationship between pressure and pore diameter (Washburn 1921).

$$r = \frac{2\sigma \cos\theta}{P_c}, \tag{1}$$

where r is the pore diameter (μm), σ is the tension at the interface between mercury and air (N/m), θ is the contact angle between mercury and the measured object varies from 135° to 142°, and P_c is the capillary pressure (MPa).

Gas permeability test

The schematic diagram of the gas permeability test device is shown in Fig. 1. During each experimental trial, compressed air was introduced into the system, where it was thoroughly purified by passing through a series of filters designed to remove oil, water, and vapour contaminants. This essential filtration process ensured that the measurements accurately reflected the permeability characteristics of the samples without interference from external factors. To quantify the airflow rate, a flowmeter was strategically installed at the exhaust end of the system, allowing for precise monitoring of the air passing through the specimen. The wood sample was oriented within

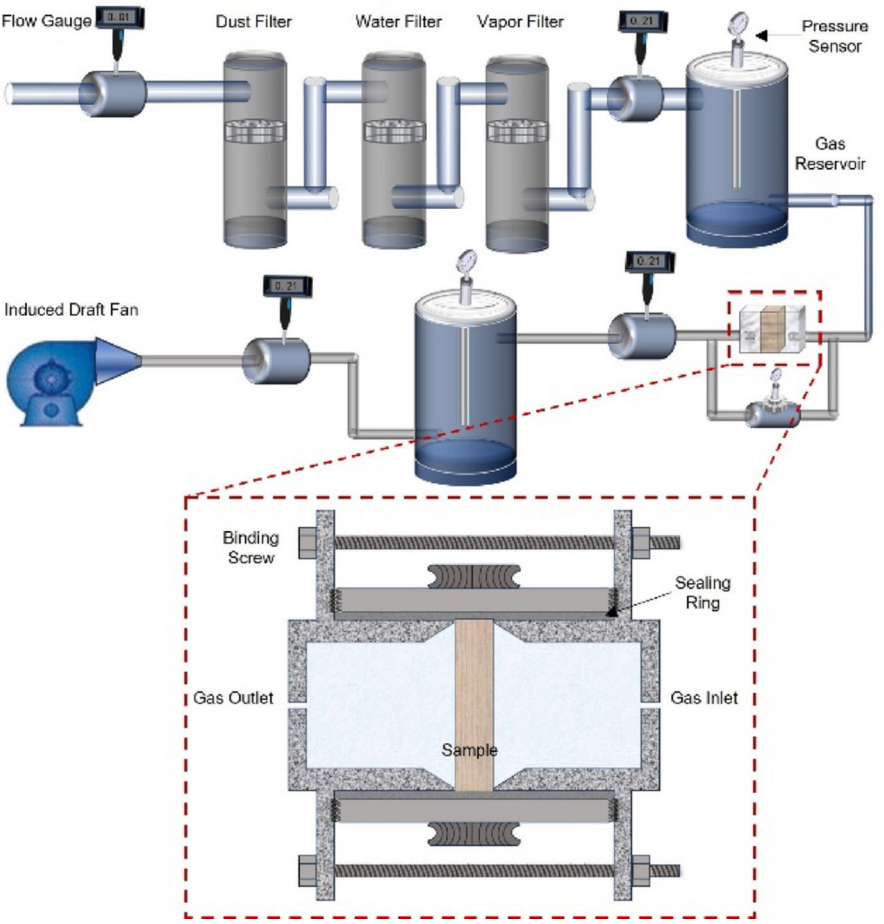

Fig. 1 The schematic diagram of gas permeability measurements

the apparatus such that its thickness direction (radial direction) was perpendicular to the airflow direction, which is more prevalent in building wood materials and wood products. After establishing a steady-state airflow condition, the gas permeability of the wood sample was determined using Darcy's law (Zhao et al. 2023).

Fractal geometric model

The pore structure of wood exhibits notable statistical self-similarity (Fan et al. 2006). This characteristic allows the wood to be conceptualized as a fractal structure that can be effectively modelled using principles of fractal theory (Tanaka and Sakai 2023; Zeng et al. 2023). To facilitate the practical application of fractal theory and streamline the modelling process, several foundational assumptions can be established:

(1) The pore structure of wood exhibits characteristics of a statistically self-similar fractal, making the theory of fractal geometry fully applicable to its analysis.
(2) The water flow inside the wood primarily occurs through the vessels for birch and oak, and through the tracheids for pine, which are distributed in the axial direction.
(3) The fluid dynamics within the wood are characterized by laminar flow (generally, $R_e < 2000$), steady-state conditions, and incompressibility, with a constant viscosity coefficient.
(4) The model does not consider the influence of environmental parameters, i.e., temperature, humidity and pressure.

According to fractal theory, the total number of pores is calculated using Eq. 2,

$$N_t = \left(\frac{r_{\max}}{r_{\min}}\right)^{D_f}, \tag{2}$$

where N_t is the total number of pores, r_{max} is the maximum pore size (nm), r_{min} is the minimum pore size (nm), and D_f is the fractal dimension, which is determined by the box-counting method (Yun et al. 2010; Li et al. 2016).

To obtain the number of pores (N) at any scale, Eq. 2 should be written in general terms. Thus, Eq. 2 is converted to Eq. 3, where r is the pore size (nm).

$$N = \left(\frac{r_{\max}}{r}\right)^{D_f}. \tag{3}$$

Generally, the maximum aperture in such materials can be measured more readily than the minimum aperture, primarily due to detection limitations associated with identifying the latter. Consequently, the r is treated as the independent variable in Eq. 3. To further analyze this relationship, Eq. 3 is differentiated (Eq. 4) with respect to the minimum aperture.

$$-\mathrm{d}N = D_f r_{\max}^{D_f} r^{-(D_f+1)} \mathrm{d}r. \tag{4}$$

The fractal dimension D_ϕ is expressed to the volume fraction of pores as follows (Eq. 5):

$$D_f = d - \frac{\ln \phi}{\ln \left(r_{\min}/r_{\max}\right)}, \tag{5}$$

where d=2 is the dimensionality for a 2D case, and ϕ is the volume fraction of pores (porosity).

Dividing Eq. 4 by Eq. 2 yields Eq. 6.

$$-\frac{\mathrm{d}N}{N_t} = D_f r_{\min}^{D_f} r^{-(D_f+1)} \mathrm{d}r. \tag{6}$$

From Eq. 6, the number of pores within the interval from r to $r+\mathrm{d}r$ can be derived. The minus sign in Eq. 6 indicates that the number of pores diminishes as pore size increases. In terms of probability theory, $f(r)$ can be interpreted as the probability density function, which meets the normalization condition across the entire range of apertures as expressed in Eq. 7,

$$\int_{r_{\min}}^{r_{\max}} f(r)\mathrm{d}r = \int_{r_{\min}}^{r_{\max}} D_f r_{\min}^{D_f} r^{-(D_f+1)} \mathrm{d}r = 1 - \left(\frac{r_{\min}}{r_{\max}}\right)^{D_f} \equiv 1. \tag{7}$$

Equation 7 is only valid when Eq. 8 is approximately equal to zero.

$$\left(\frac{r_{\min}}{r_{\max}}\right)^{D_f} \cong 0. \tag{8}$$

Fortunately, the ratio of the minimum to maximum pore size in wood is significantly less than 0.01 ($-r_{\min} << 0.01\ r_{\max}$). This indicates that the probability density function $f(r)$ is appropriately applied for this study (Plötze and Niemz 2011). Lastly, the cumulative probability $R(r)$ for pores within the range of $r_{\min}$ to r can be derived from the probability density function using Eq. 9,

$$R(r) = \int_{r_{\min}}^{r} f(r)\mathrm{d}r = \int_{r_{\min}}^{r} D_f r_{\min}^{D_f} r^{-(D_f+1)} \mathrm{d}r = 1 - \left(\frac{r_{\min}}{r}\right)^{D_f}. \tag{9}$$

Equation 9 indicates that $R=0$ as $r \to r_{\min}$ and $R=1$ as $r \to r_{\max}$. It is clear that R in Eq. 9 is in the 0 to 1 range and, thus, R approximately corresponds to a set of random numbers between zero and one. From Eq. 9, the pore size r can be expressed as Eq. 10:

$$r = \frac{r_{\min}}{(1-R)^{1/D_f}} = \frac{r_{\min}}{r_{\max}} \frac{r_{\max}}{(1-R)^{1/D_f}}. \tag{10}$$

As can be seen, Eq. 10 can determine the size of any pore, which is the geometric basis for subsequent modelling (Ferro et al. 2021; Gao et al. 2021).

Fractal geometric model

The flow rate through an individual tortuous tube is described by the modified Hagen-Poiseuille equation, as shown in Eq. 11,

$$q(r) = \frac{Gr^4 \Delta P}{\mu L_t(r)}, \tag{11}$$

where G=π/128 is the geometry factor for flow through a circular tube, DP is the pressure gradient across the length of the tubes, r is the diameter (m), μ is the dynamic liquid viscosity (m^2/s), $L_t(r)$ is the length of a tube (m), and it can be described by a fractal power law equation as follows,

$$L_t(r) = r^{1-D_T} L_0^{D_T}, \tag{12}$$

where L_0 is the representative or straight length (m), while D_T is the tortuosity fractal dimension, which ranges from 1 to 2 in two dimensions, indicating the complexity of capillary pathways for fluid movement through a medium. Clearly, $L_t(r)$ is greater than or equal to L_0. The fractal dimension associated with tortuosity can be represented by Eq. 13,

$$D_T = 1 + \frac{\ln \bar{\tau}}{\ln(L_0/\bar{r})}, \tag{13}$$

where $\bar{\tau}$is the average tortuosity of capillaries (rad/m); $\bar{r}$is the average diameter of the capillaries (m). Tortuosity of the tortuous capillary is often defined by Eq. 14,

$$\tau = L_t(r)/L_0. \tag{14}$$

The average tortuosity of capillaries can be calculated by Eq. 15,

$$\bar{\tau} = \frac{1}{2}1 + \left(\frac{1}{2}\sqrt{1-\phi} + \sqrt{1-\phi}\frac{\sqrt{\left(\frac{1}{\sqrt{1-\phi}} - 1\right)^2 + \frac{1}{4}}}{1-\sqrt{1-\phi}} \right). \tag{15}$$

The overall flow rate within the seepage flow domain can be determined by summing the individual flow rates, as shown in Eq. 16.

$$Q = \sum_{i=1}^{J} q(r_i) = \sum_{i=1}^{J} G\left(\frac{\Delta P}{L_0}\frac{A}{\mu}\right)\frac{L_0^{1-D_T}}{A} r_i^{3+D_T} = G\left(\frac{\Delta P}{L_0}\frac{A}{\mu}\right)\frac{L_0^{1-D_T}}{A}\sum_{i=1}^{J} r_i^{3+D_T}. \tag{16}$$

Compared to Darcy's law, the permeability expression is obtained as indicated in Eq. 17,

$$K = G\frac{L_0^{1-D_T}}{A}\sum_{i=1}^{J} r_i^{3+D_T}, \tag{17}$$

where Q is the total flow rate (m^3/s), A is the area (m^2), and K is the permeability (D, darcy). According to Eq. 10, Eq. 17 is rewritten as Eq. 18:

$$K = GA^{-(1+D_T)/2}\left(\frac{r_{\min}}{r_{\max}}\right)^{3+D_T} r_{\max}^{3+D_T}\sum_{i=1}^{J}\frac{1}{(1-R^i)^{(3+D_T)/D_f}}. \tag{18}$$

Equation 18 represents a probabilistic model for permeability that establishes a correlation among r_{max} and r_{min}, the fractal dimension of the pores and capillary pathways, the cross-sectional area, the probability factor (random variables), and permeability. This explicit formulation is invaluable for elucidating the relationship between structural characteristics and material properties. Once these parameters are determined through experimental methods or simulations, permeability can be accurately derived. From the perspective of porous materials and fluid seepage, the seepage flow characteristics are influenced not only by porosity and the dimensions of the maximum and minimum pore size but also, and perhaps more critically, by the distribution and arrangement of these pores. In particular, both of these aspects are effectively captured in the model proposed in this study.

Numerical algorithms

The permeability value was determined using the following procedure:

(1) Obtain porosity, pore size distribution and fractal dimension from MIP.
(2) Generate a random number, R_i, between 0 and 1.
(3) Calculate r_i using Eq. 10.
(4) If $r_i < r_{min}$ or $r_i > r_{max}$, return to step 2; otherwise, proceed to step 5.
(5) Record the value of r_i for each iteration and compute the total pore volume until the calculated volume (V_{cal}) closely matches the MIP volume, specifically until $V_{cal} = V_{MIP}$. Then, pause the calculation.
(6) Compare the MIP pore accumulation curve with the calculated curve. If the difference is less than 10%, keep all calculated data; otherwise, repeat steps 2 to 5.
(7) Calculate the fractal dimension of the pore and tortuosity using Eqs. 5 and 13.
(8) Calculate permeability from Eq. 18 and record. Then, steps 1 to 6 are repeated and the permeability is calculated in turn until the data converges.
(9) Calculate the mean and variance.

The procedure described above was implemented using software developed in MATLAB R2020b (MathWorks, Natick, MA, USA) on a Dell personal computer workstation. Compared to traditional simulation techniques, the algorithm used to determine

permeability is notably straightforward, allowing for the execution of 100,000 iterations within a matter of minutes on a standard PC. An additional advantage of this algorithm is that it provides explicit expressions for microstructural parameters, including (D_T and D_f), the total area of the cell (A), the maximum pore diameter (r_{max}), the minimum pore diameter (r_{min}), and the random variable (R). This feature significantly enhances our understanding of the physical mechanisms influencing permeability.

Results and discussion

Pore size distribution analysis based on MIP experiments

The average mercury intrusion results and the calculated pore size distributions for the three wood species are shown in Fig. 2. The pore size distribution of pine shows three regions: the macroporous range from 1 μm to 70 μm with two peak maxima at ca. 4 and 24 μm corresponding to the width of tracheids, rays and parenchyma in softwoods; the mesoporous range from 100 nm to 1 μm with a peak at 617 nm attributed to the small openings at the edges of the pits' structure; and the microporous range from 23 nm to 100 nm with a peak at 53 nm that corresponds to some microcapillary voids within the cell wall (Follrich et al. 2006).

A distinctive characteristic of the pore size distribution in birch (diffuse-porous tree) and oak (ring-porous tree) wood was observed. In the microporous range from 1 μm to 350 μm, peak maxima at 2, 7, 24 and 42 μm, and 2, 7, 13 and 22 μm, were found for birch and oak, respectively, which correspond to the width of vessels, fibres, parenchyma and rays. Similar to the pine pit's structure case in the mesoporous range, but from 50 nm to 1 μm, a single peak at 590 nm and 335 nm was found for birch and oak, respectively. Finally, in the microporous range from 3 nm to 50 nm, a peak centered at 15 nm was found for both hardwood species (Luo and Zhao 2001).

The pore structure analysis of the three types of wood studied is shown in Table 1, and the whole parameters listed there will be used to construct the geometric model. It can be seen that the porosity of pine, birch and oak was 63.1%, 54.5%, and 44.2%, respectively, and was negatively correlated with the bulk density of the material - the air-dried densities of pine, birch and oak were 450 kg/m³, 600 kg/m³, and 737 kg/m³, respectively. This was evidenced by the total volume of mercury intrusion, which was higher in pine wood compared to the other two wood species, indicating that the porosity of pine wood was larger (Wang and Wang 2014). In the MIP experimental process, mercury enters the porous structure from the three wood directions, and the increased number of flow paths naturally results in higher permeability. Furthermore, the elevated pressure during the test is likely to induce micro-cracks in the solid wood structure, contributing to the increased permeability. Additionally, MIP has certain limitations in detecting macropores. Therefore, it is recommended to determine the pore size distribution of the porous samples in conjunction with other methods based on image microscopy analysis (OLM, SEM and TEM), penetration fluid methods (N_2, He, H_2O and CO_2 sorption) or radiation methods (NMR, XCT, SAXS, SANS

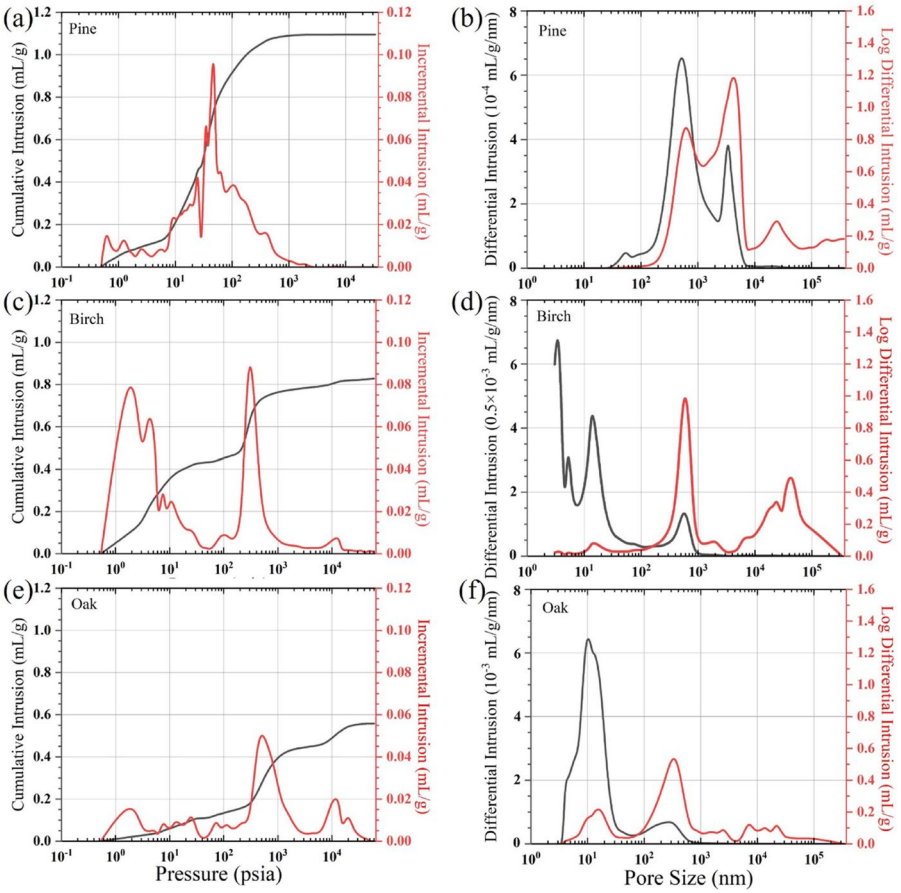

Fig. 2 Cumulative and incremental mercury intrusion as a function of the pressure (**a**, **c** and **e**) and differential (dV/dr) and log differential ($dV/d(\log r)$) mercury intrusion as a function of the pore size (**b**, **d** and **f**) for the three wood species

Table 1 Structured data from MIP experiments: weight-normalized volume V_{Hg}, porosity ϕ, minimum and maximum pore size values r_{min} and r_{max}, average pore size $\overline{r}$, the fractal dimension D_f and the tortuosity fractal dimension D_T

Wood species	V_{Hg} (mL/g)	ϕ (%)	r_{min} (nm)	r_{max} (μm)	$\overline{r}$ (μm)	D_f	D_T
pine	1.09	63.1	23.4	368	26	1.92	1.79
birch	0.82	54.5	3.0	338	14	1.95	1.84
oak	0.56	44.2	3.6	341	3.7	1.97	1.94

and TPM), for a more comprehensive characterization and complete picture of the porous material.

Structural reconstruction and permeability simulation

Figure 3 illustrates a comparison between the simulated and actual aperture distribution curves. As shown in Fig. 3, the reconstructed pore parameters exhibit a strong

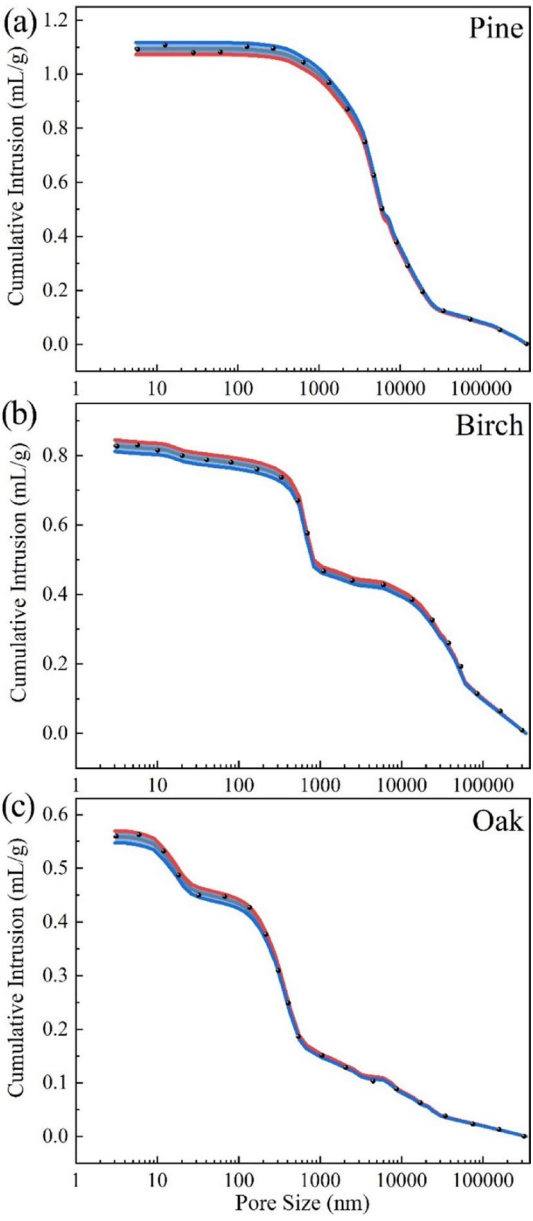

Fig. 3 Measured (line) and simulated (shaded area) values of the cumulative mercury intrusion as a function of the pore size for the three wood species

agreement with the experimental parameters obtained by MIP measurements. In a previous study, porosity or empty volume served as the sole criterion for model evaluation. Specifically, a simulated structure was considered that was consistent with the real samples when the porosity closely matched that of the actual structure. However, this approach was imprecise, as identical porosity values can arise from different pore size distributions. Consequently, in the present study, the pore size distribution was employed as the primary evaluation index, with porosity serving as an auxiliary indicator. During the initial simulations, we encountered challenges in aligning the simulated pore size distribution curves with the actual curves, leading to non-convergence of the simulated data. To address this issue, the range of the actual curve was expanded to its mean ± 2%. When the simulation values fell within this slightly broadened range, they were deemed to meet the accuracy requirements. This adjustment also holds practical significance, as the structural data of wood is not derived from one or a few samples, but rather represents a statistical aggregation of extensive data. Therefore, the data should encompass a range rather than a fixed value.

Once the structural data was established, the fractal seepage flow model could be applied. Preliminary experiments indicated that 500 iterations were sufficient to ensure the stability and accuracy of the data. Accordingly, Fig. 4 presents the simulation results after 500 iterations across different porosity levels. The results align with the expectations, as the sizes of the pores and capillary curvatures in wood exhibit a

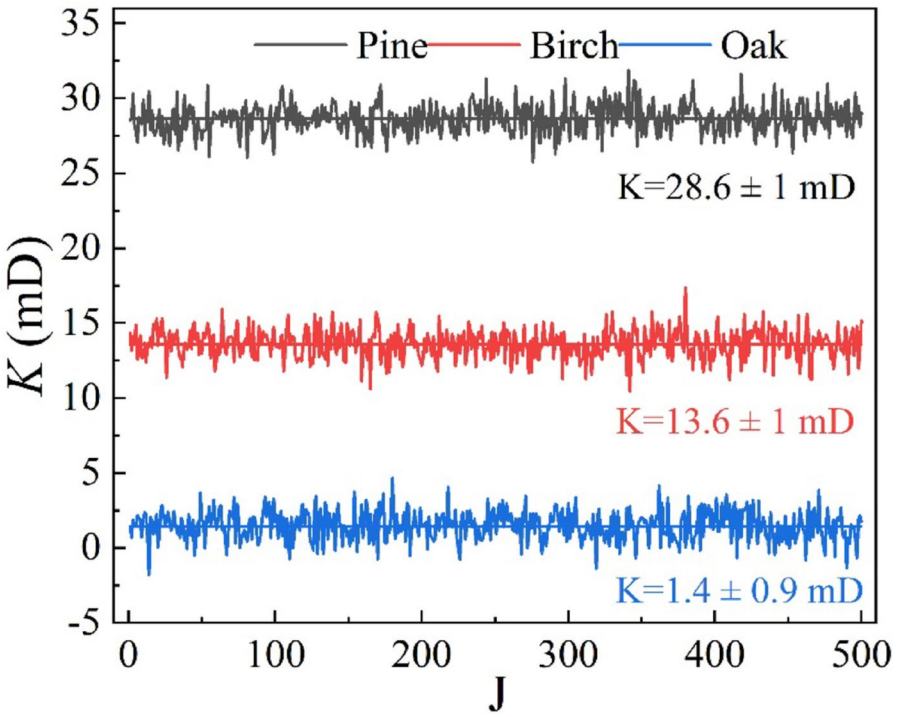

Fig. 4 Permeability simulation under J = 500 iterations for the three wood species (the values are the mean ± standard deviation)

broad range. The average permeability values for the three wood species, i.e., pine, birch and oak, were recorded as 28.6 (SD = 1.0), 13.6 (SD = 1.0), and 1.44 (SD = 0.9) mD (1 mD = $9.87 \cdot 10^{-16}$ m^2), respectively. Theoretically, the permeability of wood was not a fixed value but rather a statistical average. This model incorporates random pore size values, as indicated by the probability factor R in Eq. 9, the fractal dimension of the pores, and the capillary pathways. The simulated results correspond closely to the expected values observed in real-world scenarios.

Relationship between structure and permeability

From the perspective of porous materials, porosity is a fundamental factor influencing other material properties. This study aims to elucidate the relationship between porosity and permeability, which are two critical parameters in the characterization of building materials. Furthermore, we examined the effects of fractal dimension and tortuosity on permeability to provide a comprehensive understanding of the fluid behaviour within these building materials. The investigation was conducted by numerical simulations, which allow for the efficient generation of permeability values corresponding to varying levels of porosity and fractal dimensions. Figure 5a shows the permeability behaviour as a function of the porosity, demonstrating a strong linear correlation (R^2 = 0.992). This significant relationship indicated that as porosity increases, permeability also tends to rise. This phenomenon can be readily explained by the fact that greater porosity creates more void spaces for fluid movement, thereby enhancing the flow capacity. However, it was crucial to recognize that permeability is not solely determined by porosity. It is also significantly influenced by the pores' arrangement and shape, which were characterized by fractal dimension and tortuosity. Figure 5b shows a linear relationship between permeability and oven-dried density (R^2 = 0.997). The structural differences and inherent characteristics of wood lead to variations in permeability. As illustrated in Fig. 5b, permeability decreases with increasing oven-dried density, with coniferous wood demonstrating superior permeability compared to hardwood. The cells in coniferous wood are primarily axial cells, arranged in a regular pattern and characterized by a relatively simple structure composed of tracheids, parenchymas and rays. In contrast, hardwood exhibits a more complex structure, characterized by irregular arrangements and a more heterogeneous composition of cells like vessels, fibres, parenchyma and rays (Plötze and Niemz 2011). Moreover, hardwoods might have a different distribution of vessels, i.e., diffuse-porous trees such as birch and ring-porous trees such as oak. High-density hardwood contains a greater quantity of wood fibers, along with thicker cell walls and smaller cell cavities. Generally speaking, higher density correlates with lower permeability (Fig. 4c, R^2 = 0.994). However, there are exceptions for high porosity wood species, e.g., Norway spruce and Paulownia wood, which exhibit low permeability despite their low density. The complexity and diversity of wood structures were key factors contributing to the significant variations in permeability among different types of wood. Therefore, the application of numerical simulation methods to accurately determine permeability has become increasingly important. Figure 6 illustrates the relationship between fractal dimension, tortuosity, and permeability across various porosity levels. The analysis revealed that both fractal dimension and tortuosity

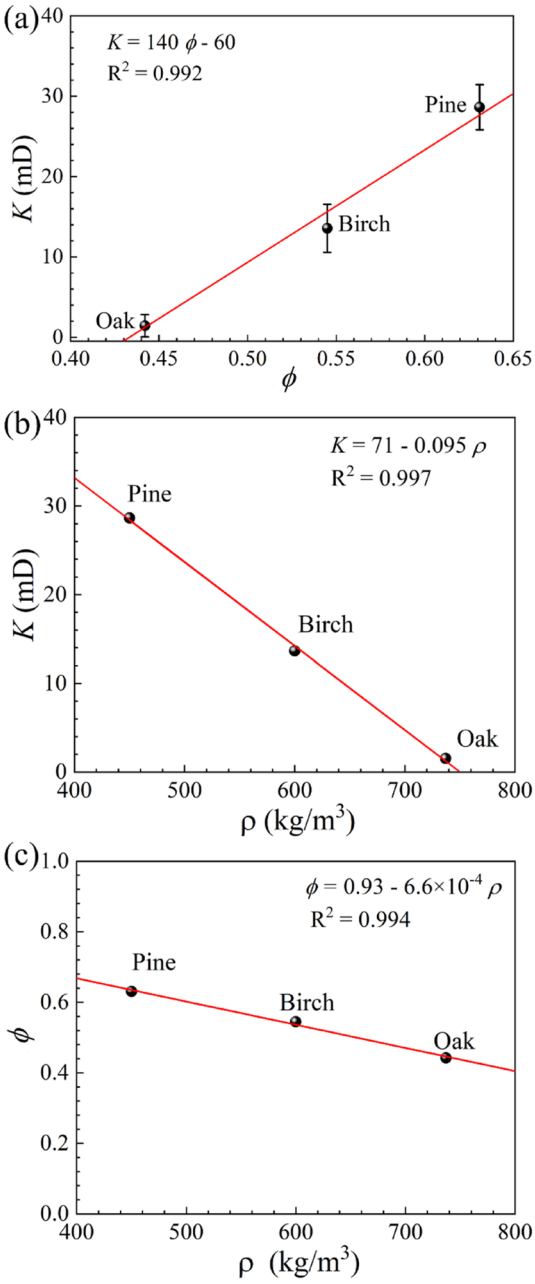

Fig. 5 Linear relationship between **a** K and ϕ, **b** K and ρ and **c** ϕ and ρ for the three wood species

fractal dimension exert a considerable impact on permeability. The fractal dimension served as a quantitative measure of structural complexity, indicating how intricately the pores were organized within the material. In contrast, tortuosity reflected the degree of curvature in the pathways that fluids must navigate through the porous structure. Notably, this study showed that permeability decreased with increasing

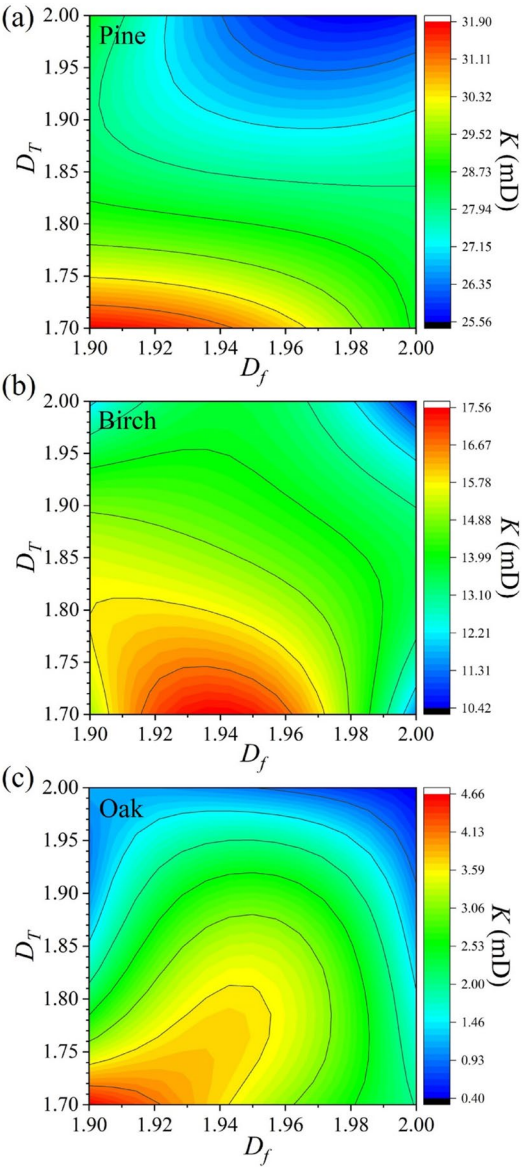

Fig. 6 Contour map showing the permeability (K) as a function of the fractal dimension (D_f) and the tortuosity fractal dimension (D_T) for the three wood species

fractal dimension and tortuosity. This decrease can be attributed to the more convoluted paths that fluids must traverse as these parameters increase, creating additional resistance to flow. Moreover, the observed trend may vary among different wood species due to inherent structural differences, underscoring the importance of biological variability in the properties of wood-based building materials (Zhang et al. 2024). These findings align well with established theories regarding mass transfer in porous media, which suggest that both structural complexity and path curvature play critical roles in determining fluid dynamics. In conclusion, this study reinforced the notion

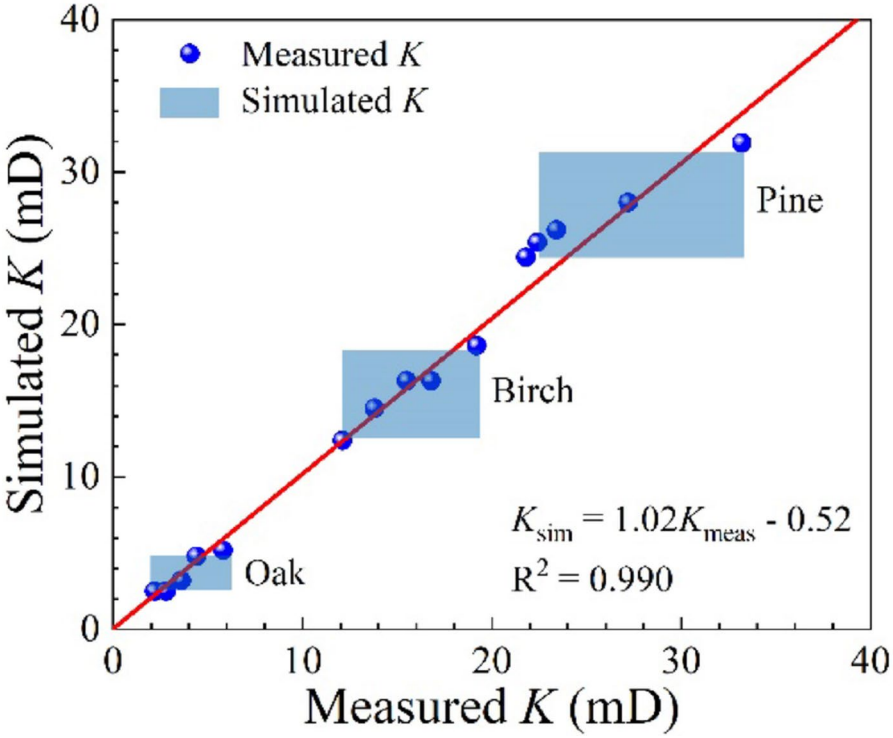

Fig. 7 Comparison between the simulated permeability and the measured permeability values for the three wood species and the linear relationship between measured and simulated permeability of the mean value

that understanding the interplay between porosity, fractal dimension, and tortuosity was vital for predicting the mass transfer behaviour of wood-based building materials. Future research should focus on exploring these relationships further, potentially incorporating experimental validation alongside numerical simulations to enhance our comprehension of fluid transport mechanisms in diverse porous structures.

The permeability verification and discussion

Figure 7 illustrates the comparison results between simulated permeability and measured permeability. The three data sets did not reasonably align, and the divergence can be attributed to three primary factors. First, the discrepancies were largely due to inherent variations in wood properties. It was well documented that wood exhibited considerable variability, even among different segments of the same specimen (Emaminasab et al. 2017; Ananías et al. 2023). There is some fluctuation in the measured values, however, they remained within the expected range. Even the largest fluctuation, observed in the pine, was within just 10 mD. Such variability underscores the complexity of wood as a natural material, influenced by factors such as growth conditions, wood species, and anatomical structure. Second, the differences

in calculation methods and parameters used may also contribute to these variations. The computation of permeability inherently relies on model calculations, which can introduce discrepancies based on the assumptions made during the modelling process. For instance, the methodology used to derive the fractal dimension, which plays a critical role in calculating permeability, may have introduced additional variability. The choice of parameters, such as those related to the pore's shape and arrangement, further exemplifies how methodological differences can impact the final results. Finally, variations in the accuracy of experimental methods may account for one of the reasons for the discrepancies observed. Currently, there is a lack of standardized equipment and techniques for conducting permeability tests, which can lead to inconsistencies in measurement outcomes. Different laboratories might employ different methods, resulting in divergent data even when testing similar samples (Khlewee et al. 2023). In summary, while the simulation results suggested that the model proposed in this study was acceptable, the accuracy can be enhanced through several avenues. Optimizing calculation parameters, enriching structural characterization methods, and improving experimental protocols will contribute to more reliable permeability assessments. Future research should focus on standardizing methodologies and exploring the influence of wood-based material characteristics on permeability to further validate and refine the model.

Conclusion

This study investigated a novel fractal analytical model for assessing permeability in wood. Grounded in fractal theory, the proposed model utilized MIP data to derive an explicit expression for permeability that effectively captured the structural characteristics of wood. The model integrated key structural parameters of wood, including minimum and maximum pore size values, pore size distribution, porosity, fractal dimension, and tortuosity fractal dimension. By accounting for these factors, the model provided a comprehensive framework for understanding how the internal architecture– anatomy - of wood influences its permeability.

Validation of the simulated permeability values produced by the model was conducted through experimental comparisons, demonstrating a strong correlation between the simulated and measured results. Specifically, the permeability measurements for the three wood species analyzed under specific orientation conditions, i.e., pine, birch and oak, were 28.6 mD, 13.6 mD, and 1.4 mD, respectively. These findings indicated that the model not only accurately reflected the permeability of different wood species but also served as a reliable tool for predicting such properties based on structural information. The simulation results further revealed a clear relationship between permeability and various structural parameters. Specifically, permeability tended to increase with higher porosity and decrease with both fractal dimension and tortuosity fractal dimension. Notably, the influence of porosity on permeability was found to be more significant than that of the latter two parameters, highlighting the critical role of porosity in determining the flow characteristics of wood.

The model presented in this paper offered an innovative approach to establishing the relationship between the structural features of wood and its physical properties.

It will be essential to optimize the model parameters further and expand the sample size to enhance the reliability and accuracy of the predictions. Future research should also explore the application of this model across a broader range of wood species and in different environmental conditions, i.e., temperature and relative humidity, to validate its robustness and generalizability.

Supplementary Information The online version contains supplementary material available at https://doi.org/10.1007/s00226-025-01680-4.

Acknowledgements This work was supported by the National Natural Science Foundation of China (No. 32271786) and the Fundamental Research Funds for the Central Universities (No. 2572023AW54).

Author contributions All authors contributed to the study's conception and design. Material preparation, data collection and analysis were performed by Zhipeng Zhu, Jingyao Zhao and Antoni Sánchez-Ferrer. Zhipeng Zhu wrote the first draft of the manuscript. Jingyao Zhao and Antoni Sánchez-Ferrer contributed to the revising of the manuscript. All authors read and approved the final manuscript.

Funding Open Access funding enabled and organized by Projekt DEAL.

Data availability No datasets were generated or analysed during the current study.

Declarations

Competing interests The authors have no competing interests to declare that are relevant to the content of this article.

References

Acosta AP, Barbosa KT, Xavier da Silva AA et al (2023) Vacuum infusion as a novel method to determine wood permeability. Eur J Wood Wood Prod 81:33–44. https://doi.org/10.1007/s00107-022-01887-3

Ai W, Duval H, Pierre F et al (2017a) Characterization of wood micromorphology from gas permeability measurements. Microfluid Nanofluid. https://doi.org/10.1007/s10404-017-1936-1

Ai W, Duval H, Pierre F et al (2017b) A novel device to measure gaseous permeability over a wide range of pressures: characterisation of slip flow for Norway spruce, European beech, and wood-based materials. Holzforschung 71:147–162. https://doi.org/10.1515/hf-2015-0264

Ananías RA, Leandro-Zúñiga L, Pérez-Peña N et al (2023) Transverse permeability in *Eucalyptus* nitens wood specimens. Wood Mater Sci Eng 18: 1035–1042. https://doi.org/10.1080/17480272.2022.2102436

Brozovsky J, Nocente A, Rüther P (2023) Modelling and validation of hygrothermal conditions in the air gap behind wood cladding and BIPV in the Building envelope. Build Environ 228. https://doi.org/10.1016/j.buildenv.2022.109917

Burridge HC, Pini R, Shah SMK et al (2021) Identifying efficient transport pathways in early-wood timber: Insights from 3D X-ray CT imaging of softwood in the presence of flow. Transp Porous Media 136: 813–830. https://doi.org/10.1007/s11242-020-01540-8

Dang Mao N, Almeida G, Thi Mai Loan N et al (2021) A critical review of current imaging techniques to investigate water transfers in wood and biosourced materials. Transp Porous Media 137:21–61. https://doi.org/10.1007/s11242-020-01538-2

Di Trobiani JA, Malfait WJ, Wernery J (2023) Turning waste into insulation– A new sustainable thermal insulation board based on wheat bran and banana peels. Build Environ. https://doi.org/10.1016/j.buildenv.2023.110740

El Assaad M, Colinart T, Lecompte T (2023) Thermal conductivity assessment of moist Building insulation material using a heat flow meter apparatus. Build Environ 234. https://doi.org/10.1016/j.buildenv.2023.110184

Emaminasab M, Tarmian A, Oladi R et al (2017) Fluid permeability in poplar tension and normal wood in relation to ray and vessel properties. Wood Sci Technol 51: 261–272. https://doi.org/10.1007/s00226-016-0860-y

Fan L, Hu Y, Tian T et al (2006) The prediction of effective thermal conductivities perpendicular to the fibres of wood using a fractal model and an improved transient measurement technique. Int J Heat Mass Transf 49:4116–4123. https://doi.org/10.1016/j.ijheatmasstransfer.2006.03.027

Ferro F, Arroyo F, Rodrigues E et al (2021) Investigation of pore size distribution by mercury intrusion porosimetry (MIP) technique applied on different OSB panels. BioResources 16:6661–6668. https://doi.org/10.15376/biores.16.4.6661-6668

Follrich J, Mueller U, Gindl W (2006) Effects of thermal modification on the adhesion between spruce wood (*Picea abies Karst*.) and a thermoplastic polymer. Holzforschung 64: 373–376. https://doi.org/10.1007/s00107-006-0107-y

Gao Y, Wu K, Yuan Q (2021) Limited fractal behavior in cement paste upon mercury intrusion porosimetry test: Analysis and models. Constr Build Mater. https://doi.org/10.1016/j.conbuildmat.2020.122231

Hargittai I (2024) Remembering Benoit Mandelbrot on his centennial—his fractal geometry changed our view of nature. Struct Chem 35:1657–1661. https://doi.org/10.1007/s11224-024-02290-9

Hu X, Zhang H, Yu H (2023) Numerical simulation study on the hygrothermal performance of building exterior walls under dynamic wind-driven rain condition. Build Simul 17: 207–221. https://doi.org/10.1007/s12273-023-1076-3

Jang E, Yuk J, Kang C (2020) An experimental study on change of gas permeability depending on pore structures in three species (*Hinoki*, *Douglas fir*, and *Hemlock*) of softwood. J Wood Sci. https://doi.org/10.1186/s10086-020-01925-9

Khlewee M, DeSisto WJ, Bousfield DW (2023) Prediction of non-isothermal polymer penetration into porous layers. Ind Eng Chem Res 62:11178–11185. https://doi.org/10.1021/acs.iecr.3c00782

Kvist P, Therning A, Gebäck T et al (2017) Lattice Boltzmann simulations of diffusion through native and steam-exploded softwood bordered pits. Wood Sci Technol 51: 1261–1276. https://doi.org/10.1007/s00226-017-0938-1

Kvist P, Geback T, Rasmuson A (2020) A multi-scale model for diffusion of large molecules in steam-exploded wood. Wood Sci Technol 54:821–835. https://doi.org/10.1007/s00226-020-01185-2

Li P, Tao Y, Wu Q (2016) A three-dimensional void reconstruction method for analyzing fractal dimensions of void volume in wood-strand composites. Holzforschung 70:377–382. https://doi.org/10.1515/hf-2015-0024

Li X, Zhou W, Duanmu L (2020) Research on air infiltration predictive models for residential building at different pressure. Build Simul 14:737–748. https://doi.org/10.1007/s12273-020-0685-3

Lü X, Lu T, Kibert C et al (2017) A dynamic modelling approach for simulating climate change impact on energy and hygrothermal performances of wood buildings. Build Simul 11:497–506. https://doi.org/10.1007/s12273-017-0421-9

Luo W, Zhao G (2001) Pore structure of cell wall of wood and transport processes of substance. J Beijing Univ 23:85–89. https://doi.org/10.13332/j.1000-1522.2001.02.022

Marynowicz A, Kucharczyk A (2021) Determination of the water absorption and water diffusion coefficients by means of infrared thermography measurements. Measurement. https://doi.org/10.1016/j.measurement.2021.110054

Merlier L, Frayssinet L, Johannes K et al (2019) On the impact of local microclimate on building performance simulation. Part II: effect of external conditions on the dynamic thermal behavior of buildings. Build Simul 12: 747–757. https://doi.org/10.1007/s12273-019-0508-6

Multon S, Verdier J, Villain G et al (2022) Non-destructive measurements for the evaluation of the air permeability of concrete structures. Measurement. https://doi.org/10.1016/j.measurement.2022.111204
Plötze M, Niemz P (2011) Porosity and pore size distribution of different wood types as determined by mercury intrusion porosimetry. Eur J Wood Wood Prod 69: 649–657. https://doi.org/10.1007/s00107-010-0504-0
Portal NW, van Schijndel AWM, Kalagasidis AS (2013) The multiphysics modeling of heat and moisture induced stress and strain of historic Building materials and artefacts. Build Simul 7:217–227. https://doi.org/10.1007/s12273-013-0153-4
Rahiminejad M, Räber V, Ghazi Wakili K et al (2024) Wooden basements; hygrothermal performance analysis using in-field measurements and numerical simulations. Build Environ. https://doi.org/10.1016/j.buildenv.2024.111475
Rezaeyan A, Pipich V, Ma J et al (2022) Predicting fluid flow regime, permeability, and diffusivity in mudrocks from multiscale pore characterisation. Transp Porous Media 141: 201–229. https://doi.org/10.1007/s11242-021-01717-9
Sanchez-Ferrer A, Böger T, Engelhardt M et al (2023) Wood-water interactions of primers to enhance wood-polyurethane bonding performance. Wood Sci Technol 58: 135–160. https://doi.org/10.1007/s00226-023-01508-z
Tanaka S, Sakai Y (2023) Estimation of actual pore-size distribution by inverse analysis of mercury intrusion. Constr Build Mater 366. https://doi.org/10.1016/j.conbuildmat.2022.130208
Tarmian A, Mastouri A (2018) Water-repellent efficiency of thermally modified wood as affected by its permeability. J Res 29:859–867. https://doi.org/10.1007/s11676-017-0495-3
Wang Z, Wang X (2014) Research progress of multi-scale pore structure and characterization methods of wood. Scientia Silvae Sinicae 50:123–133. https://doi.org/10.11707/j.1001-7488.20141017
Washburn E (1921) Note on a method of determining the distribution of pore sizes in a porous material. PNAS 7:115–116. https://doi.org/10.1073/pnas.7.4.115
Yu Q, Dai Z, Zhang Z et al (2019) Estimation of sandstone permeability with SEM images based on fractal theory. Transp Porous Media 126: 701–712. https://doi.org/10.1007/s11242-018-1167-2
Yuan Y, Doonechaly N, Rahman S (2016) An analytical model of apparent gas permeability for tight porous media. Transp Porous Media 111:193–214. https://doi.org/10.1007/s11242-015-0589-3
Yun M, Yu B, Lu J et al (2010) Fractal analysis of Herschel-Bulkley fluid flow in porous media. Int J Heat Mass Transf 53:3570–3574. https://doi.org/10.1016/j.ijheatmasstransfer.2010.04.020
Zeng L, Zhu J, Zhao Y et al (2023) Pore structure characteristics and permeability analysis of natural anhydrite with various water/unhydrite ratios based on mercury intrusion porosimetry. Constr Build Mater. https://doi.org/10.1016/j.conbuildmat.2023.132422
Zhang G, Wu H, Liu J et al (2022) Dynamic performance and energy efficiency of reflective and insulative composite coating on building exterior wall. Build Simul 16: 2245–2259. https://doi.org/10.1007/s12273-022-0932-x
Zhang R, Zhang M, Zhao H et al (2024) Revealing the behavior and mechanism of surfactant-assisted liquid permeability in Poplar wood. Ind Crops Prod. https://doi.org/10.1016/j.indcrop.2023.117998
Zhao J, Yang L, Cai Y (2020) Combining mercury intrusion porosimetry and fractal theory to determine the porous characteristics of wood. Wood Sci Technol 55: 109–124. https://doi.org/10.1007/s00226-020-01243-9
Zhao J, Li L, Lv P et al (2023) A comprehensive evaluation of axial gas permeability in wood using XCT imaging. Wood Sci Technol 57: 33–50. https://doi.org/10.1007/s00226-022-01449-z
Zheng S, Song X, Duanmu L et al (2024) Comparison of models to predict air infiltration rate of buildings with different surrounding environments. Build Simul 17: 1007–1021. https://doi.org/10.1007/s12273-024-1118-5
Zhu Y, Guo S, Liang W (2024a) A literature review investigating the impact of temperature and humidity on volatile organic compound emissions from building materials. Build Environ. https://doi.org/10.1016/j.buildenv.2024.111845
Zhu Z, Song X, Chi X et al (2024b) Characterization of hygrothermal, gas pressure and stress characteristics for poplar wood during unilateral surface densification. Constr Build Mater. https://doi.org/10.1016/j.conbuildmat.2024.137099

Authors and Affiliations

Zhipeng Zhu[1] · Feifan Lv[1] · Jiajun Lv[1] · Riwei Huang[1] · Chiyang Mao[1] · Yingchun Cai[1] · Wanli Cheng[1] · Antoni Sánchez-Ferrer[2] · Jingyao Zhao[1]

✉ Antoni Sánchez-Ferrer
sanchez@hfm.tum.de

✉ Jingyao Zhao
zjy_20180328@nefu.edu.cn

[1] Key Laboratory of Bio-based Material Science and Technology of Ministry of Education, Northeast Forestry University, Harbin 150040, China

[2] Wood Materials Science, TUM School of Engineering and Design, Wood Research Institute of Munich (HFM), Technical University of Munich, Winzererstr. 45, 80797 Munich, Germany